DRUG DELIVERY
2022, VOL. 29, NO. 1, 548–560
https://doi.org/10.1080/10717544.2022.2036873

Taylor & Francis
Taylor & Francis Group

ORIGINAL ARTICLE

Construction and performance of exendin-4-loaded chitosan–PLGA microspheres for enhancing implant osseointegration in type 2 diabetic rats

Shaojie Shi[a,b]*, Shuang Song[c]*, Xiangdong Liu[a]*, Guoqiang Zhao[a], Feng Ding[a], Wenshuang Zhao[a], Sijia Zhang[a], Yingliang Song[a] and Wei Ma[a]

[a]Department of Oral Implants, School of Stomatology, State Key Laboratory of Military Stomatology & National Clinical Research Center for Oral Diseases & Shaanxi Engineering Research Center for Dental Materials and Advanced Manufacture, The Fourth Military Medical University, Xi'an, China; [b]Department of Oral Surgery, 920th Hospital of Joint Logistics Support Force, Kunming, China; [c]Department of Implant Dentistry, College of Stomatology, Xi'an Jiaotong University, Xi'an, China

ABSTRACT

The updating and optimization of drug delivery systems is critical for better *in vivo* behaviors of drugs, as well as for improving impaired implant osseointegration in diabetes. Numerous studies have reported the benefits of exendin-4 on diabetic bone, with the potential to enhance osseointegration in diabetes. To construct an appropriate sustained-release system of exendin-4 targeting implant osseointegration in diabetes, this study fabricated exendin-4-loaded microspheres using poly(lactic-co-glycolic acid) (PLGA) and chitosan. The morphology, size, encapsulation efficiency, and drug release behavior of microspheres were investigated. The bioactivity of drug-loaded microspheres on cell proliferation and osteogenic differentiation of diabetic BMSCs was investigated to examine the pharmacologic action of exendin-4 loaded into chitosan–PLGA microspheres. Further, the influence of microspheres on osseointegration was evaluated using type 2 diabetes mellitus (T2DM) rat implant model. After 4 weeks, the samples were evaluated by radiological and histological analysis. The results of *in vitro* experiments showed that the prepared exendin-4-loaded chitosan–PLGA microspheres have good properties as a drug delivery system, and the chitosan could improve the encapsulation efficiency and drug release of PLGA microspheres. In addition, exendin-4-loaded microspheres could enhance the proliferation and osteogenic differentiation of diabetic BMSCs. The results of *in vivo* experiments showed the exendin-4-loaded microspheres significantly improved the impaired osseointegration and bone formation around implants in T2DM rats without affecting blood glucose levels. Thus, the local application of exendin-4-loaded chitosan–PLGA microspheres might be a promising therapeutic strategy for improving the efficacy of dental implants in T2DM individuals.

ARTICLE HISTORY
Received 23 December 2021
Revised 24 January 2022
Accepted 25 January 2022

KEYWORDS
Type 2 diabetes mellitus; exendin-4; poly(lactic-co-glycolic acid); chitosan; microspheres; osseointegration

1. Introduction

The type 2 diabetes mellitus (T2DM) patients face a higher risk of missing teeth than the non-diabetic patients (López-Gómez et al., 2020), and have a large requirement for dental implant treatment. Unfortunately, diabetes can damage the implant osseointegration (Niang et al., 2011), which may be related to the adverse effect of diabetes on bone metabolism. It is currently accepted that some systemic drugs can be beneficial to bone metabolism and promote osseointegration (Apostu et al., 2017), such as parathyroid hormone (Jiang et al., 2018). However, diabetes could compromise the efficacy of this anabolic drug to enhance osseointegration (Kuchler et al., 2011). Therefore, the more appropriate drug strategy must be found to improve the osseointegration in diabetes.

Exendin-4, a classic GLP-1 receptor agonist, is a new hypoglycemic drug, which has beneficial effects on bone in diabetic individuals (Nissen et al., 2019). The application of exenatide (synthetic of exendin-4) can alleviate the impairment of diabetes on bone formation and improve the trabecular bone mass in severe T2DM mice (Pereira et al., 2017). Further, additional study indicated that exendin-4 can promote the osteogenic differentiation and inhibit the adipose differentiation of BMSCs (Meng et al., 2016), and induce the migration of BMSCs (Wang et al., 2017), which is conducive to the bone regeneration process. Moreover, our previous work also demonstrated the promotion of exendin-4 on osteogenic differentiation of adipose-derived stem cells and bone defect repair (Deng et al., 2019). These positive effects of exendin-4 on bone could be a potential means of promoting osseointegration in diabetes.

Considering the extensive distribution of GLP-1 receptor and the limited half-life of drug in diabetic individuals (Schiellerup et al., 2019), an ideal local delivery strategy should be adopted to maintain an appropriated concentration of exendin-4 around implants. Previous studies have suggested that poly(lactic-co-glycolic acid) (PLGA)-based microspheres could be an attractive sustained-release carrier for exendin-4 (Chien et al., 2015; Wang et al., 2017). At present, the only

CONTACT Yingliang Song songyingliang@163.com; Wei Ma 4138088@qq.com Department of Oral Implants, School of Stomatology, The Fourth Military Medical University, Shaanxi, Xi'an 710032, China
*These authors contributed equally to this work.

approved long-acting sustained-release formulation of exendin-4, Bydureon®, is made from PLGA materials, showing the advantages and safety of PLGA as the drug carrier of exendin-4 (Li et al., 2021). Significantly, it has been reported that chitosan can improve the drug delivery properties of PLGA microspheres (Badran et al., 2018), but there is currently no exendin-4-loaded sustained-release carrier made of PLGA and chitosan. Moreover, the PLGA-based microspheres could also be used as the delivery vehicle for protein around titanium implants (Wang et al., 2019). Therefore, this study is designed to construct a superior drug delivery system of exendin-4 based on PLGA and chitosan, and investigate the influence of exendin-4 on osteointegration in T2DM rats.

2. Materials and methods

2.1. Materials

PLGA (75:25, Mw = 1.5 w) was purchased from Ruixi Biological Technology (Xi'an, China); chitosan was purchased from Sigma (St. Louis, MO); exendin-4 was purchased from MCE (Kenner, LA); rats exendin-4 ELISA-Kit was purchased from Jianglaibio (Shanghai, China); cell counting kit-8 (CCK-8) was purchased from DOJINDO Laboratories (Kumamoto, Japan); BCIP/NBT working solution was purchased from Beyotime Biotech (Shanghai, China); alkaline phosphatase assay kit was purchased from Jiancheng (Nanjing, China); alizarin red S staining was purchased from Solarbio (Beijing, China); titanium implants (length of 5 mm and diameter of 2 mm) was purchased from Kontour Medica (Xi' an, China); alizarin red S and calcein was purchased from Sigma-Aldrich (St. Louis, MO).

2.2. Animal models and cell culture

The experiments were approved by the Ethics Committee of School of Stomatology, the Fourth Military Medical University (2020-k9-010). The Guidelines of the Institutional Animal Care and Use Committee of China was followed. A total of 50 eight-week-old male Sprague-Dawley (SD) rats (Chengdu Dossy Experimental Animals Co., Ltd., Chengdu, China) were acquired for this study. Each rat was kept in its own cage in exactly the same environment (25 °C, 55% humidity, 12 hours of light alternating with 12 hours of darkness). Thirty rats were randomly selected and induced into the T2DM models by a high-sucrose and high-fat diet and streptozotocin (STZ, Sigma, St. Louis, MO) (30 mg/kg). The blood glucose levels were measured from the tail vein 72 h after STZ injection. The rats with blood glucose level higher than 16.7 mmol/L were included in the next experiments. One normal rat and one diabetic rat were euthanized and their pancreas were taken for observation with HE staining.

The BMSCs were isolated from the femurs of normal and T2DM rat for subsequent study, respectively. The rats were sacrificed with excessive anesthesia and soaked in 75% alcohol for 5 min. The internal marrow of femur was exposed at both ends and flushed out from end to end with α-MEM culture medium supplemented with 10% FBS and 1% antibiotics. The suspension was transferred into the cell culture dishes, and incubated at 37 °C in an incubator containing 5% CO_2. The P3 cells were used for the next experiments. The BMSCs surface-characterized expression markers of CD29, CD34, CD44, CD45, CD90 and CD105 (Biolegend, San Diego, CA) were analyzed by the flow cytometry assay.

2.3. Fabrication of the exendin-4-loaded microspheres

This study fabricated the exendin-4-loaded chitosan–PLGA microspheres by the solvent evaporation method (Figure 1(A)). Briefly, 1 mg of exendin-4 (MedCemExpress, South Brunswick Township, NJ) was dissolved in 0.5 mL of distilled water to obtain the internal water phase (W1). One hundred milligrams of PLGA (75:25, Mw = 1.5 w, Ruixi Biological Technology, Xi'an, China) was dissolved in 10 mL of methylene chloride as organic phase (O). One gram of polyvinyl alcohol (PVA) was added to 100 mL of acetic acid solution (1%, v/v) containing different concentrations (0, 0.1%, 0.2%, and 0.3%, w/v) of chitosan as the external water phase (W2). The W1 phase was added into the O phase, and homogenized with the high-speed homogenizing emulsifier (FLUKO, Shanghai, China) at 20,000 rpm for 1 min in the ice bath to form primary emulsions (W1/O). The W1/O emulsions were quickly added dropwise to the W2 phase, and then emulsified for 3 min at 12,000 rpm to obtain the coarse double emulsions (W1/O/W2). Afterward, the resulting mixture was stirred overnight (300 rpm) at room temperature to volatilize the organic components fully. The solidified microspheres were collected by centrifugation at 7674×*g* for 15 min, and washed with distilled water. The microspheres were vacuum freeze dried for 25 h, and stored at −20 °C to maintain the morphology. The microspheres containing different concentrations (0, 0.1%, 0.2%, and 0.3%, w/v) of chitosan were named as M0, M1, M2, and M3, respectively.

2.4. The morphology, size, drug loading, and drug release in vitro of the microspheres

The morphology of microspheres was observed by a scanning electron microscope (SEM, Phenom LE, Eindhoven, Netherlands). The particle sizes of microspheres were evaluated by the laser diffraction particle size analyzer (Beckman Coulter, Brea, CA). The size uniformity was expressed as the Span value:

$$\text{Span} = \frac{(\text{Dv}, 90\%) - (\text{Dv}, 10\%)}{\text{Dv}, 50\%}.$$

where Dv,10%, Dv,50%, and Dv,90% represented the volume size diameters of the particles at 10%, 50%, and 90% of the cumulative volume, respectively.

To evaluate the loading efficiency and encapsulation efficiency, 5 mg of microspheres were dispersed in 10 mL of 0.1 mol/L NaOH solution (containing 5% SDS). The suspension was incubated at 110 rpm under 37 °C for 24 h. After complete degradation, the microspheres were centrifuged at 1000×*g* for 20 min and the supernatant was

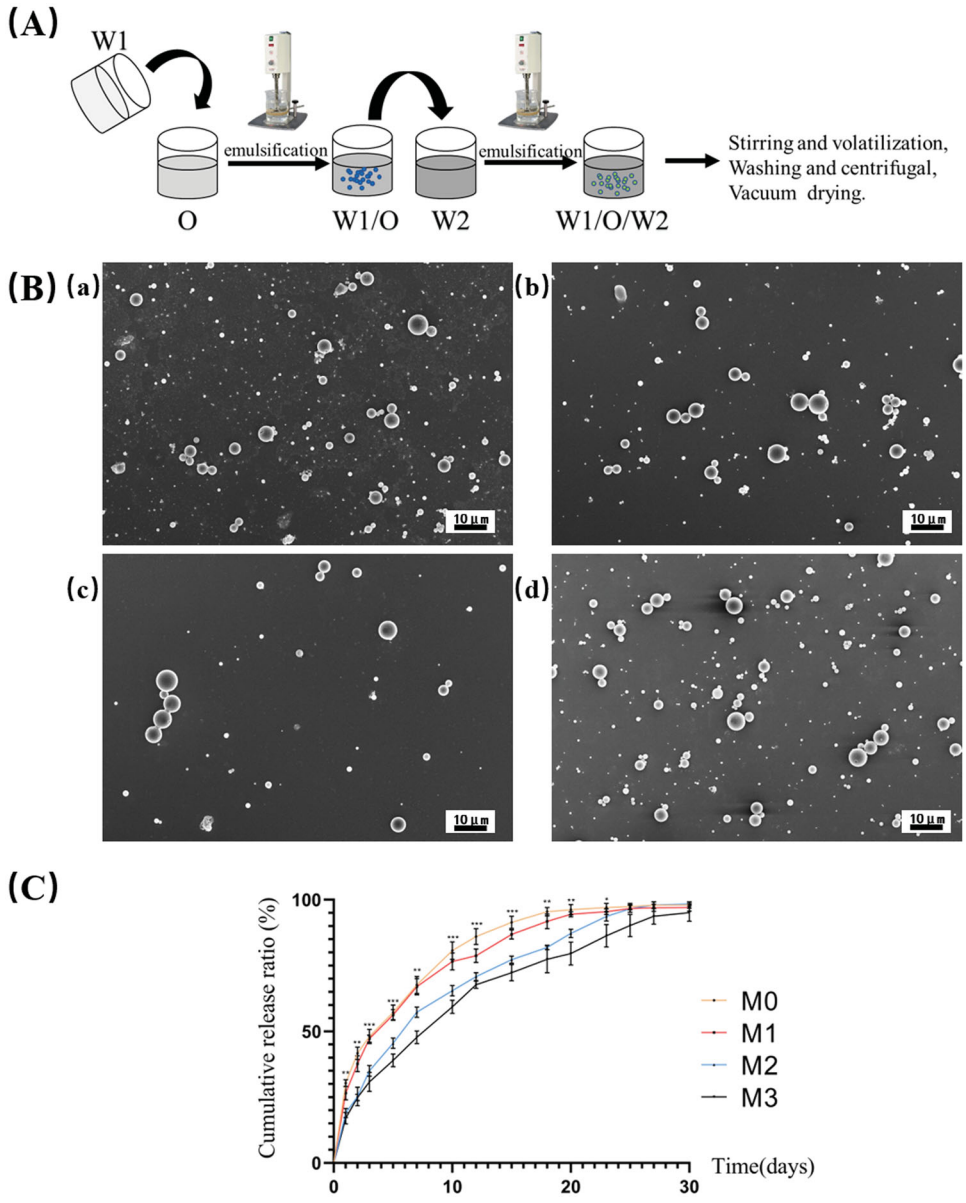

Figure 1. The preparation and characterization of drug-loaded microspheres. (A) The schematic diagram of preparation process of drug-loaded microspheres. (B) SEM images of microspheres. (C) *In vitro* release profiles of microspheres. (a) M0, (b) M1, (c) M2, and (d) M3. Scale bar = 10 μm. $^{*}p<.05$; $^{**}p<.01$.

collected. The amount of exendin-4 was measured by the enzyme-linked immunosorbent assay (ELISA) method. The loading efficiency (%) and encapsulation efficiency (%) were calculated as follows:

$$\text{Loading efficiency } (\%) = \frac{\text{amount of drug in microspheres}}{\text{mass of the microspheres}}$$

$$\text{Encapsulation efficiency } (\%) = \frac{\text{actual amount of drug encapsulated in microspheres}}{\text{initial amount of drug used}}$$

The drug release behavior of these productions was explored. Ten milligrams of microspheres were immersed in 10 mL of PBS solution (pH = 7.4), and shaken at 110 rpm under 37 °C for 30 days. At predetermined time (1, 2, 3, 5, 7, 10, 12, 15, 18, 20, 23, 25, 27, and 30 days), the drug delivery system was centrifuged at 3824×*g* for 5 min. The supernatant was taken and replaced with equivalent amount of fresh PBS. All these samples were examined by the ELISA method and the sustained-release curve was plotted.

2.5. The bioactivity of exendin-4 released from the drug-loaded microspheres

The M2 was prepared for the follow-up experiments after comparing the drug loading and release behaviors.

The effect of drug loaded into the microspheres on cell proliferation was detected by the CCK-8 (DOJINDO Laboratories, Kumamoto, Japan). Three groups were analyzed: the (1) normal group: normal BMSCs cultured in α-MEM medium; the (2) T2DM group: diabetic BMSCs cultured in α-MEM medium; the (3) exendin-4 group: diabetic BMSCs cultured in medium containing the supernatant collected from the drug release study *in vitro*. The BMSCs were seeded in 96-well plates (3000 cells/well) and cultured. The cell proliferation was measured on day 1, 3, 5, and 7. The old medium was changed with 100 μL of fresh medium and

10 μL of CCK8 solution. After incubation for 4 h at 37 °C, the optical density (OD) values were measured at 450 nm.

The effect of drug loaded into the microspheres on osteogenic differentiation of diabetic BMSCs was investigated. Three groups were divided as above. The BMSCs were seeded in six-well plates (2×10^6 cells/well). These BMSCs were induced in osteogenic differentiation medium, and the medium was changed every three days. After seven days, these cells were stained with BCIP/NBT working solution (Beyotime Biotech, Shanghai, China). The quantitative analysis of the alkaline phosphatase (ALP) activity was performed using the alkaline phosphatase assay kit (Jiancheng, Nanjing, China) in accordance with the manufacturer's instructions. After 21 days, the mineralized extracellular matrix was stained by alizarin red S staining (Solarbio, Beijing, China). Then, the mineralized nodules were extracted by cetylpyridinium chloride for one hour and semi-quantified by measuring the OD values at 620 nm. All above staining outcomes were observed under a microscope (Olympus IX70, Tokyo, Japan).

2.6. Surgical procedures and postoperative management

The experiment consists of four groups ($n = 8$ in each group): the (1) normal group: normal rats receiving only implant placement, the (2) T2DM group, T2DM rats receiving only implant placement, the (3) blank carrier group, T2DM rats receiving blank microspheres injection and subsequent implant placement, and the (4) drug-loaded carrier group, T2DM rats receiving drug-loaded microspheres injection and subsequent implant placement. Diabetic rats were randomly assigned to the latter three groups and the order of treatment was randomized to eliminate confounding factors. This study adopted titanium implants with a length of 5 mm and a diameter of 2 mm. The rats received the general anesthesia with 1% pentobarbital sodium (45 mg/kg rat weight), and the local analgesia with Primacaine® (Pierre Rolland, Bordeaux, France). Afterwards, a longitudinal incision on the lateral side of the knee joint was performed. Then, the hole was created in the femoral condyles parallel to the long axis of the femora. Ten milligrams of microspheres were applied into the holes. Then, the implants were inserted into the holes in the same location on both sides meticulously. Afterwards, the incisions were sutured in layers carefully and benzylpenicillin sodium was administered for five days after surgery. The blood glucose was continuously monitored at the same time every day for 20 days after surgery. At the twentieth and tenth day before sacrifice, a sequence of alizarin red S (30 mg/kg) and calcein (20 mg/kg) (Sigma-Aldrich, St. Louis, MO) was administered intraperitoneally, respectively. The samples with infection were excluded from the study. After 4 weeks, these rats were sacrificed and the femurs containing implants were harvested.

Each experiment evaluating the osseointegration and bone formation followed were repeated at least in triplicate, so the result analysis required 12 specimens per group, representing six rats in each group. In order to prevent the failure risk from affecting the result analysis, two rats were added to each group based on this sample size. The grouping of rats was known and sealed by one of the experimenters, who did not participate in the experimental process and data analysis. The grouping was not notified to others until the data analysis was complete.

2.7. Evaluation of osseointegration and bone around implants

2.7.1. Micro-CT analysis

The specimens were fixed overnight in 70% ethanol ($n = 5$ in each group). Then, specimens were shaped to an appropriate size and put into the microcomputed tomography (Siemens Inveon, Erlangen, Germany). The bone structure around implants was scanned and acquired with a high-resolution mode. The region of interest (ROI) was defined as the trabecular region within a distance of 200 μm away from the implant surface. The scanned images were reconstructed into three-dimensional structures. All related morphometric parameters within the ROI were evaluated, including the bone volume percentage (BV/TV, %), trabecular separation (Tb. Sp, μm), trabecular thickness (Tb. Th, μm), and trabecular number (Tb. N, 1/μm).

2.7.2. Sequential fluorescence labeling test

After gradient dehydration through a series of ethanol (75–100%), specimens ($n = 4$ in each group) were infiltrated in methyl methacrylate and then embedded in poly-methylmethacrylate resin. Each specimen was cut through the center of the implant parallel to its long axis using a hard tissue slicer (Leica SP1600, Nussloch, Germany). The thickness of each section should be about 300 μm, which can prevent the implant shedding due to the too thin section. Then, the slice was grinded and polished to a sheet of 30 μm. The undecalcified sections were directly observed under the confocal laser scanning microscopy (OLYMPUS, Tokyo, Japan) with different wavelengths of spectral excitation fluorescence. The mineral apposition rate (MAR) was measured to indicate the speed of osteoid mineralization during the observation period.

2.7.3. Histological evaluation

The undecalcified sections were stained with Methylene Blue acid fuchsin staining (VG staining) and toluidine blue staining ($n = 3$ in each group). The parameters including the bone-to-implant contact (BIC) and the bone area (BA) were assessed with Image J software (National Institutes of Health, Bethesda, MD). The BIC was measured as the percentage of the contact interface between the bone and implant to the total length of the implant surface. The BA represented the proportion of bone tissue in the area around the implant.

2.8. Statistical analysis

All data were presented as mean ± standard deviation (SD) and analyzed with the special software SPSS v25.0 (SPSS, Chicago, IL). The drug loading among groups and the amount of drug released

from each group at predetermined time were compared among groups with one-way analysis of variance (ANOVA). The results of blood glucose between normal and diabetic rats were applied *t*-test to perform statistical analysis. The comparison of osseointegration and bone formation outcomes among groups was performed with ANOVA, followed by multiple comparisons using LSD method. When the variance of each group is not uniform, the Bonferroni post hoc adjustment test was performed for the multiple comparisons. The charts were made with GraphPad Prism 5 (GraphPad Software, La Jolla, CA). The level of significance was set as .05.

3. Results

3.1. The characterization of drug delivery system

The SEM results showed that these microspheres presented the smooth spherical shape (Figure 1(B)). The particle size and Span value of M0 were 1.526 ± 0.248 μm and 0.438 ± 0.023, respectively. While the particle size and Span value of M1, M2, and M3 were 2.271 ± 0.302 μm, 2.939 ± 1.553 μm and 4.258 ± 2.692 μm, 0.356 ± 0.058, 1.503 ± 0.083 and 1.846 ± 0.061, respectively, showing the increased particle size and decreased distribution uniformity with the addition of chitosan.

The loading efficiency of M0 was the highest (0.22 ± 0.01%) ($p < .01$), and that of M3 was the smallest (0.11 ± 0.01%) ($p < .05$). While there was no significant difference between the loading efficiency of M1 (0.15 ± 0.01%) and M2 (0.14 ± 0.01%) ($p > .05$). The encapsulation efficiency of M0 was 45.33 ± 2.03%, while that of M1, M2, and M3 was 45.49 ± 1.69%, 53.97 ± 1.78%, and 54.71 ± 1.94%, respectively. The encapsulation efficiency of M2 and M3 was both higher than that of M0 and M1 ($p < .01$). There was no significant difference in the encapsulation efficiency between the M2 and M3, and between the M0 and M1 ($p > .05$).

The various drug release characteristics *in vitro* of these productions are shown in Figure 1(C). The results showed these microspheres all exhibited a nonlinear drug release process, including an initial rapid release stage and followed a slower release stage. With the addition of chitosan, the initial burst release effect of drug-loaded microspheres decreased significantly, and the subsequent release process became prolonged.

The M2 was prepared for the follow-up experiments. As the encapsulation efficiency of M2 was significantly higher, drug release behavior of M2 was more stable and slower than M1 and M0. Furthermore, compared with M2, the encapsulation rate and drug release characteristics of M3 did not change significantly with the increasing of chitosan concentration.

3.2. Biological activity of exendin-4 released from the drug-loaded microspheres in vitro

The expressions of CD29, CD44, CD90, CD105, CD34, and CD45 in T2DM cells and normal cells were: 98.7%, 98.4%, 99.6%, 99.9%, 1.1% and 1.4%, 99.2%, 99.3%, 99.9%, 99.8%, 1.1% and 2.8%, respectively (Figure 2(A)). It was confirmed that the surface markers of stem cells were positively expressed and the BMSCs were isolated successfully.

As shown in Figure 2(B), the cell proliferation of T2DM group was less than that of normal group, both at day 5 ($p < .01$) and day 7 ($p < .05$). The cell proliferation in the exendin-4 group was significantly higher than that in the T2DM group at day 5 ($p < .05$).

After seven days of osteogenic induction, the ALP secretion of diabetic BMSCs was less than the normal BMSCs, while the ALP secretion in the exendin-4 group was more than the T2DM group (Figure 2(C)). Quantitative analysis also revealed a lower ALP activity in T2DM group than the normal group ($p < .01$), but the drug intervention increased the ALP activity of diabetic BMSCs ($p < .05$). After 21 days, the calcium nodule of diabetic BMSCs was significantly less than the normal BMSCs, while the drug intervention can significantly increase the mineralized nodule deposition (Figure 2(D)).

3.3. Animal model establishment and postoperative observation

After four weeks of special diet, the rats in the modeling group became significantly fatter than normal group (Figure 3(A)). After modeling, the blood glucose levels of all the diabetic rats were significantly higher than normal rats and met the modeling criteria (Figure 3(B)). The morphology of normal pancreas was regular and the boundary of islets was clear. While in the diabetic rats, abnormal proliferation of pancreatic tissues was observed, and islet boundary became chaotic (Figure 3(C)).

After implant surgery process (Figure 3(D)), three rats in the T2DM group, two rats in the blank carrier group and two rats in the drug-loaded carrier group had local infection in the operation area, all of which were excluded from the study. There were no obvious signs of infection in the normal group. The daily blood glucose monitoring within 20 days after surgery is shown in Figure 3(E). The blood glucose of diabetic rats was significantly higher than normal rats ($p < .05$). Compared with T2DM group, the blood glucose of the drug-loaded carrier group did not exhibit any significant differences ($p > .05$).

3.4. Micro-CT analysis of bone mass and microstructure

The bone mass around implants in the T2DM group was significantly less than the normal group, while the bone mass in the drug-loaded carrier group was significantly more than the T2DM group (Figure 4). The analysis of bone microstructure in ROI showed the lower BV/TV, Tb. Th and higher Tb. Sp in T2DM group than the normal group ($p < .01$). However, after drug-loaded microspheres were applied around implants, BV/TV and Tb. N in the drug-loaded carrier group were higher than the T2DM group ($p < .05$), and the Tb. Sp in drug-loaded carrier group was lower than the T2DM group ($p < .05$).

3.5. Evaluation of new bone formation around implants

The fluorescence labeling lines around implants were detected by the laser confocal microscope (Figure 5), showing the bone formation at different periods. The new bone formation area around implants in the T2DM group was less

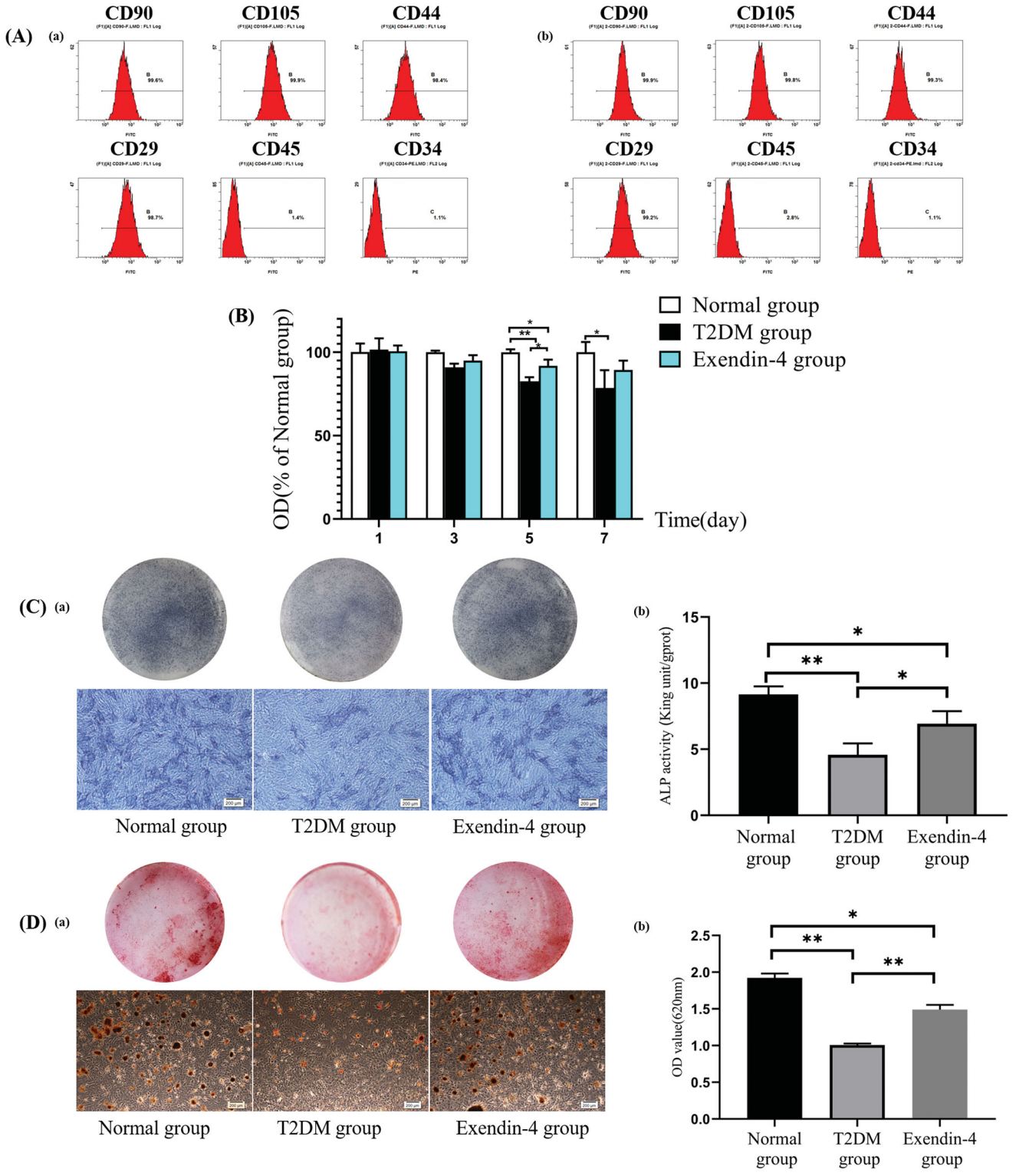

Figure 2. The biological activity assay of drug-loaded microspheres. (A) Expression of (a) diabetic and (b) normal BMSCs surface markers. (B) Cell proliferation. (C) After seven days, the (a) BCIP/NBT staining for alkaline phosphatase, and the (b) quantitative comparison of ALP activity. (D) After 21 days, the (a) alizarin red staining for mineralized nodules, and the (b) semi-quantitative comparison of alizarin red staining. Scale bar = 200 μm. *p<.05; **p<.01.

than that in the normal group, while the local application of drug-loaded microspheres could significantly increase the new bone formation in T2DM rats. The MAR in normal group was the highest (2.11 ± 0.48 μm/d) (p< .01). The MAR in the drug-loaded carrier group was 1.93 ± 0.63 μm/d, which was higher than the T2DM group and blank carrier group (1.21 ± 0.49 μm/d and 1.16 ± 0.14 μm/d) (p< .05).

3.6. Histological analysis of osseointegration and bone around implants

It could be seen that the bone tissue around implants stained by two methods was red and blue-purple, respectively (Figure 6(A)). In normal group, massive levels of bone trabecula structure were in contact with the surface of the implants. The results showed a significant worse bone mass

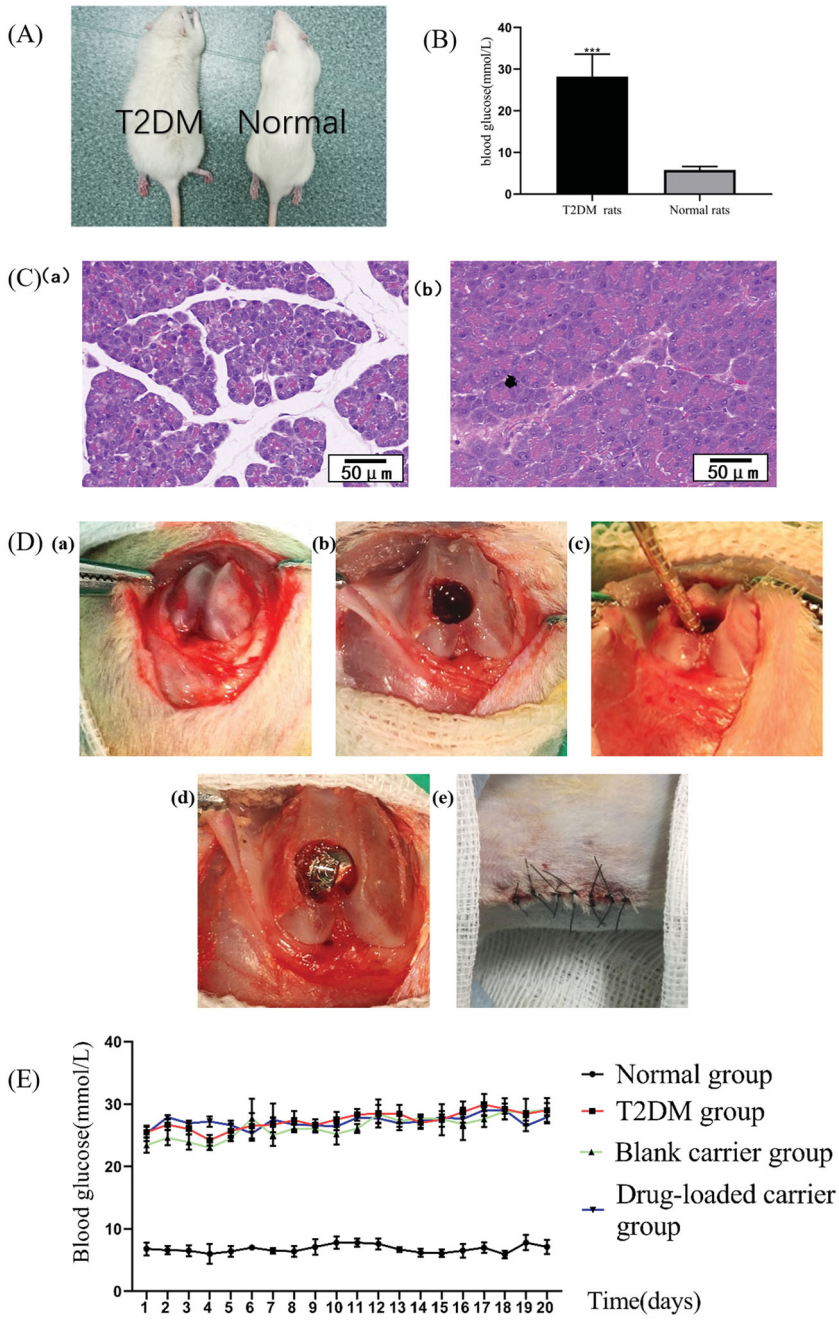

Figure 3. Animal model establishment, intraoperative and postoperative observation. The (A) general appearance and the (B) blood glucose levels of the T2DM and normal rats. (C) HE staining for pancreatic tissue of the (a) normal rats and the (b) T2DM rats. Scale bar = 50 μm. (D) Surgical procedure. (E) Daily blood glucose monitoring within 20 days after operation. ***$p<.001$.

around implants in the T2DM group than the normal group. Compared with the T2DM group, the bone mass around implants in the drug-loaded carrier group was significantly improved, and the trabecular bone was thicker and denser. The analysis results indicated that the BIC in T2DM rats was significantly less than the normal group ($p< .01$), while exendin-4-loaded microspheres significantly improved the BIC in the T2DM rats ($p< .05$). The same trend was observed in BA around implants, indicating the bone tissue around implants in drug-loaded microspheres group was significantly better than the T2DM group.

4. Discussion

Although previous studies have demonstrated the advantages of exendin-4 in bone metabolism (Deng et al., 2021; Liang et al., 2021), the influence of exendin-4 on osseointegration still remains unclear in diabetic individuals. In order to investigate the role of exendin-4 on peri-implant bone, an appropriate local administration route should be applied. In this study, exendin-4-loaded chitosan–PLGA microspheres were constructed, and the potential of exendin-4 to enhance the bone formation and osseointegration in T2DM rats was investigated using this drug delivery system.

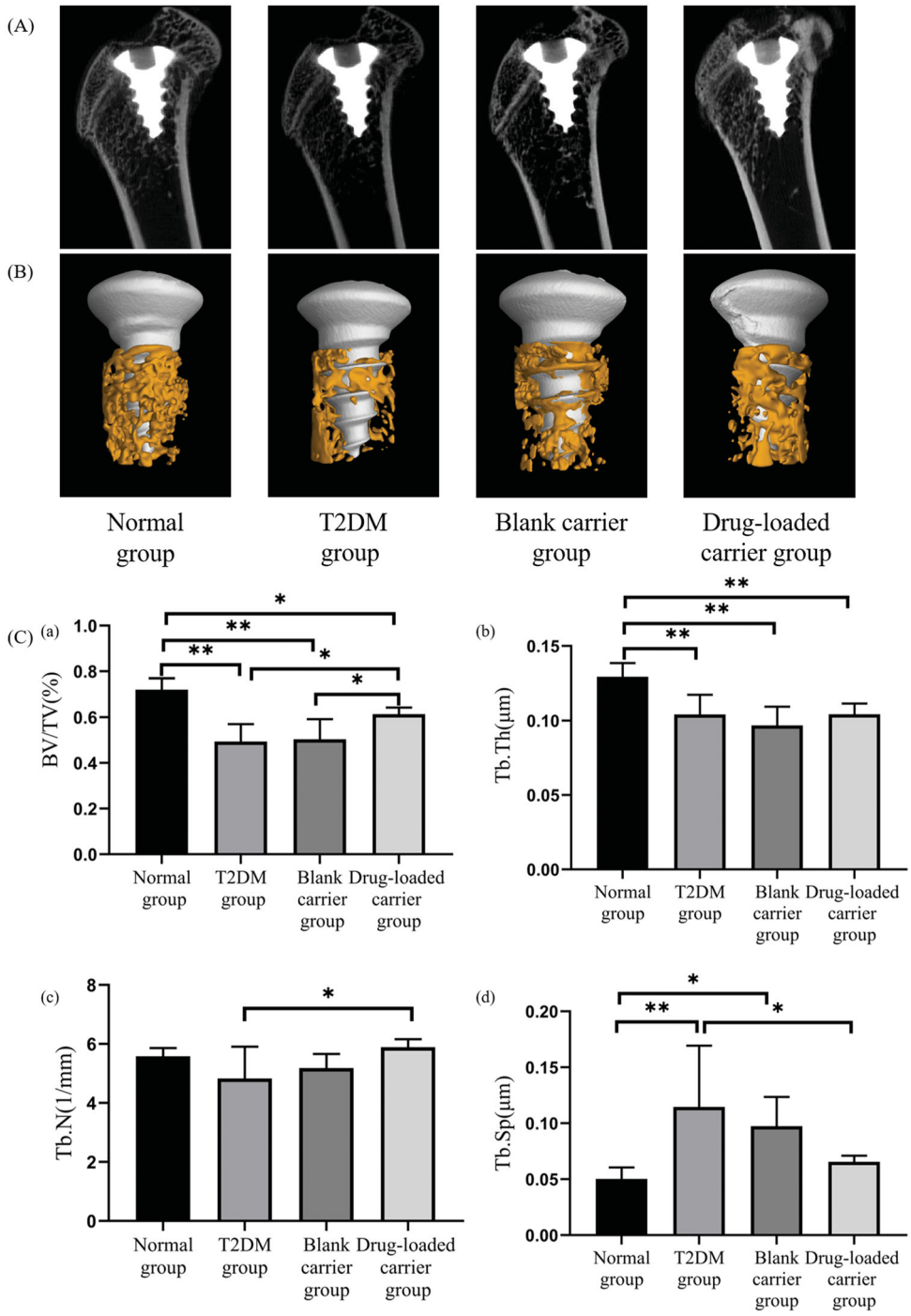

Figure 4. The micro-CT images of the specimens. (A) Two-dimensional images of specimens. (B) The reconstruction of the ROI around implants. (C) The statistical data of BV/TV, Tb. Th, Tb. N, and Tb. Sp in each group. BV/TV: percentage of bone volume; Tb. Th: trabecular thickness; Tb. N: trabecular number; Tb. Sp: trabecular separation. $^{*}p < .05$; $^{**}p < .01$.

This study selected the solvent evaporation method (Figure 1(A)) to construct the drug-loaded PLGA microspheres, referring to previous studies (Chen et al., 2017; Abd El Hady et al., 2019), which has been proved to be more suitable for wrapping exendin-4 than other methods, including the solvent extraction and cosolvent method (Qi et al., 2014). In addition, it has been reported that chitosan can improve the performance of PLGA microsphere as drug delivery system (Chen et al., 2016). Thus, different concentrations of chitosan were used for the preparation of exendin-4-loaded PLGA microspheres. The results of SEM indicated that chitosan did not significantly affect the smooth spherical surface morphology of the PLGA microspheres (Figure 1(B)). Further, the larger mean particle size and lower particle size uniformity were obtained after chitosan incorporation. Another study has also reported that chitosan could increase the particle size of PLGA microspheres (Ahmad et al., 2020), which can promote the adhesion and reduce the clearance rate of microspheres at the target site.

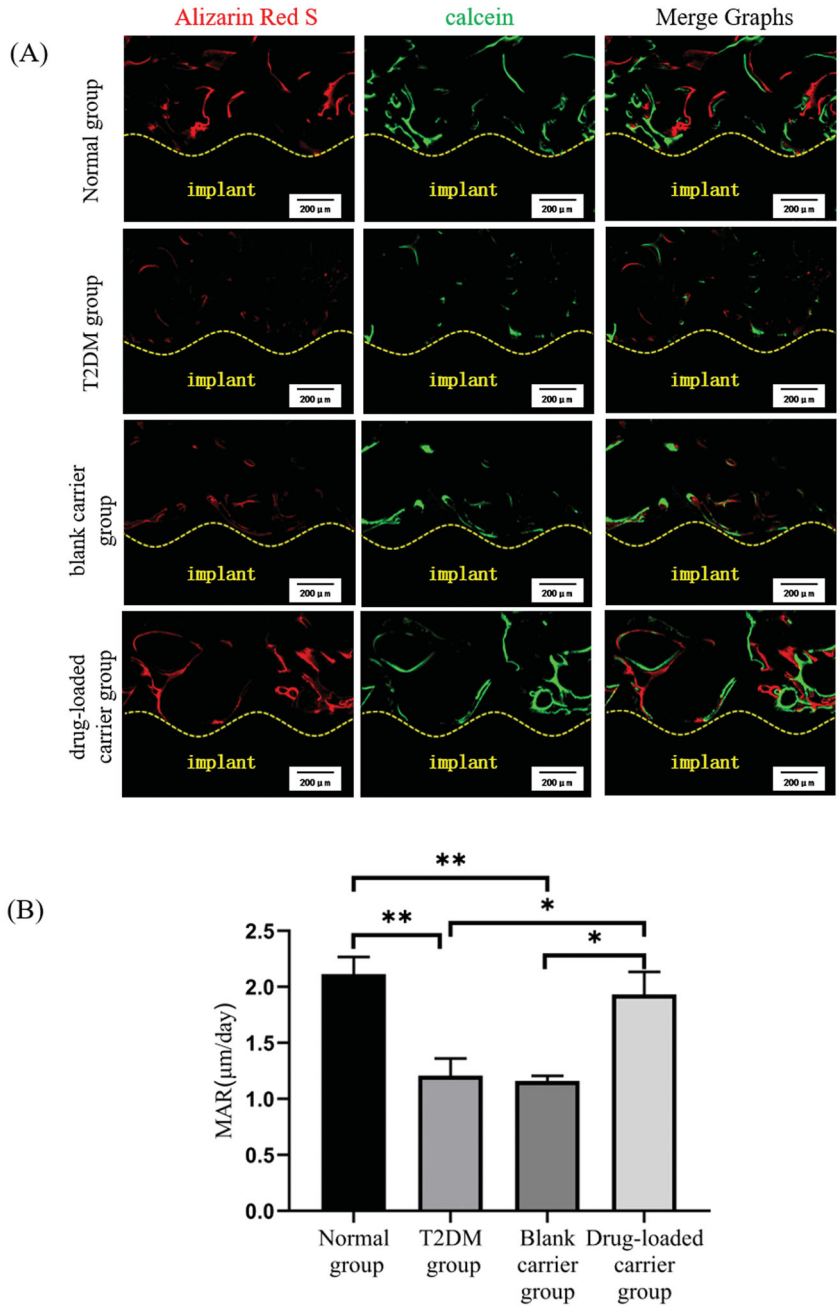

Figure 5. The assessment of new bone formation by the double fluorescence labeling method. (A) The image of the double fluorescence labeling observed under confocal laser scanning microscopy. (B) The mineral deposition rates. Scale bar = 200 μm. *$p < .05$; **$p < .01$.

The drug loading capacity and release kinetics are crucial properties of the drug sustained-release carriers. This study showed the addition of chitosan can reduce the loading efficiency and increase the encapsulation efficiency of microspheres. The decrease in loading efficiency with the increase of chitosan concentration may be because the overall mass of microspheres increased after the addition of chitosan, while the amount of drug added during the process remained the same. The encapsulation efficiency represents the ratio of actual drug loading efficiency to theoretical drug loading efficiency, which can better suggest the drug loading capacity of the carrier. Arafa et al. (2020) also reported a higher encapsulation efficiency of chitosan-modified PLGA nanoparticles than that of PLGA alone. The improved drug loading capacity may be related to the influence of chitosan on the solubility and surface charge number density of PLGA (Taghavi et al., 2017; Takeuchi et al., 2017). The releasing curve demonstrated that these productions can release exendin-4 during the observed period (Figure 1(C)). The microspheres without chitosan showed the fastest release rate and about a 30% burst release within the first 24 hours. By contrast, a prolonged release was found for microspheres containing chitosan, and the release rate was most dependent on the concentration of chitosan. In particular, the initial burst effect is reduced by chitosan, which was consistent with previous research (Lu et al., 2019). The change of initial drug release could be related to the enhanced adsorption of drugs on the surface of chitosan-modified microspheres. The

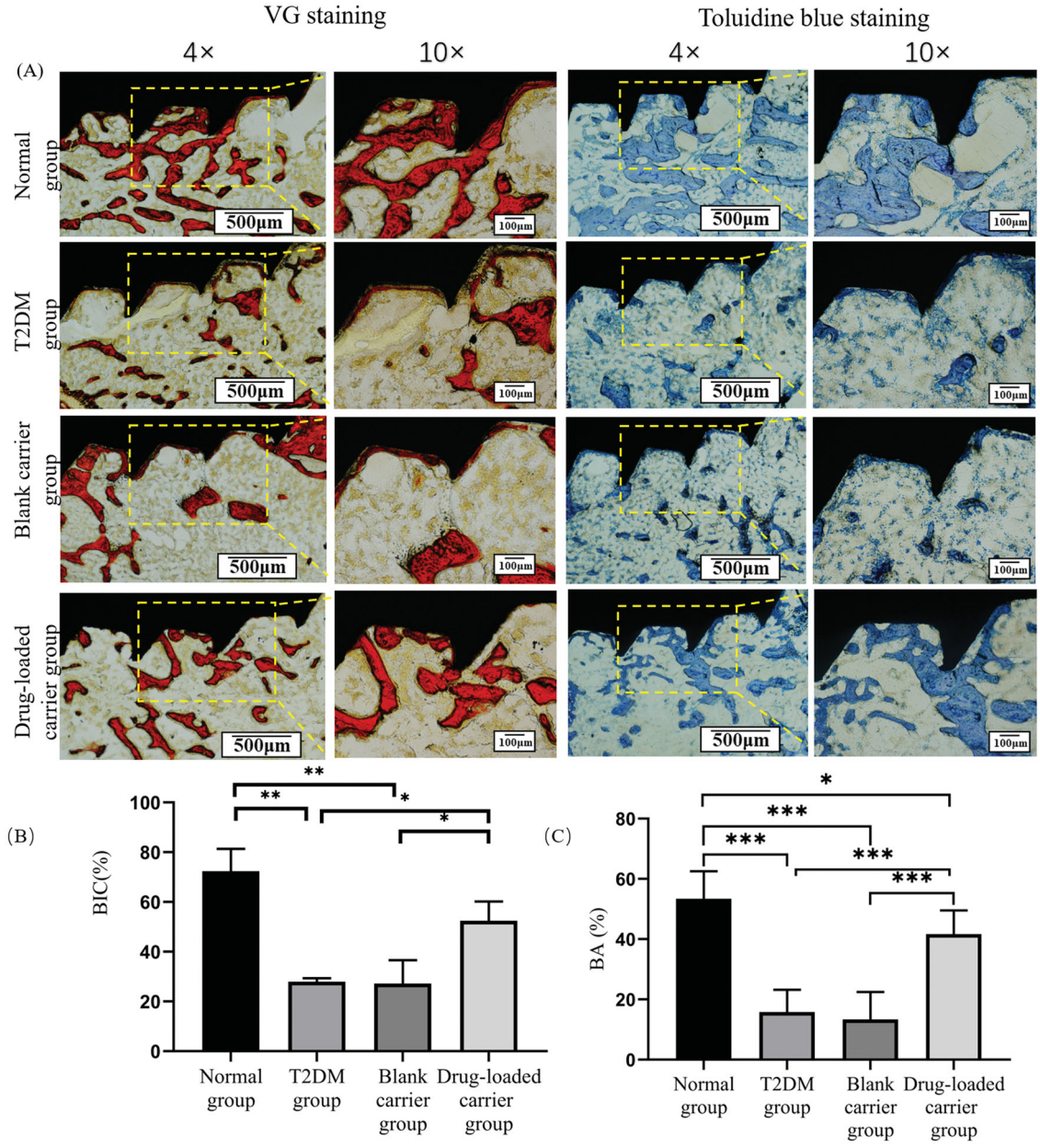

Figure 6. (A) The images of the undecalcified sections stained with VG staining and toluidine blue staining under light microscopy. (B) Statistical results of the BIC; (C) Statistical results of BA. Scale bar = 500 μm (magnification ×4). Scale bar = 100 μm (magnification ×10). $^{*}p<.05$; $^{**}p<.01$; $^{***}p<.001$.

more stable subsequent sustained release process might be related to the influence of chitosan on the interior structure of PLGA microspheres, which can slow down the diffusion rate of the encapsulated molecules (Sanna et al., 2015). The process of drug release from microspheres is a combination of diffusion and degradation (Pola et al., 2019). These results indicated that the chitosan can act as a barrier material to delay the diffusion and degradation of PLGA microspheres for longer duration of action.

The bioactivity *in vitro* of this drug delivery system and the pharmacologic action of exendin-4 loaded into microspheres was evaluated by affecting the proliferation and osteogenic differentiation of diabetic BMSCs. This study showed exendin-4 released from the microspheres could improve the proliferation ability of diabetic BMSCs (Figure 2(B)). The reason might be that exendin-4 can protect mitochondrial function by eliminating ROS and regulating the anti-apoptotic proteins (Zhou et al., 2015). A previous study also proved that GLP-1 can act on the receptor to improve cell proliferation of BMSCs (Sanz et al., 2010). In this work, the ALP secretion of the BMSCs in T2DM group decreased significantly than the normal group, showing the damaged early osteogenesis in diabetes. However, drug intervention can reverse this trend, which was attributed to the positive effects of exendin-4 on osteogenesis (Figure 2(C)). To further observe the enhancement of exendin-4 on the osteogenesis, the alizarin red staining results showed that the number of calcium nodules in the T2DM group was the smallest but significantly improved by drug intervention (Figure 2(D)). Another study also suggested that exendin-4 can facilitate the osteogenic differentiation of BMSCs in ovariectomized rats (Sun et al., 2016). Combined with these results, the present study demonstrated that exendin-4 released from

the microspheres exhibited good biocompatibility to facilitate the proliferation and osteogenic differentiation of diabetic BMSCs.

As shown in Figure 3(A–C), this study induced T2DM rat model successfully by the high-fat/high-sugar diet plus low-dose STZ injection method (King et al., 2016). After modeling, T2DM rats showed a worse bone microarchitecture around implants than normal rats (Figure 4), most of which came down to the influence of diabetes on bone metabolism. It has been well-established that T2DM is associated with the increased bone trabecular porosity and decreased cortical bone mass (Lecka-Czernik, 2017). What was worse, diabetes could impair the fracture healing process. A study reported the significantly smaller calcified callus and worse mechanical properties of new bone in diabetic rats during fracture healing (Guo et al., 2020), which was related to the lower osteogenic capability. Further, the diabetes will inhibit the bone remodeling process around dental implants (Coelho et al., 2018). Similar results can be observed in this study, showing that T2DM rats faced a higher risk of postoperative infection and failure of implants than normal rats. Therefore, it is necessary to ameliorate the adverse effects of diabetes on bone around implants to improve the clinical efficacy of dental implants in T2DM individuals.

This study was the first to use exendin-4-loaded chitosan–PLGA microspheres in bone tissues around implants in T2DM rats and suggested the local application of exendin-4 can enhance the bone formation around implants. The fluorescence labeling area and MAR in the drug-loaded carrier group increased significantly than the T2DM group, indicating the strengthened bone regeneration (Figure 5). The reason might be that the adverse effect of diabetes on the bone formation was efficiently relieved by exendin-4 released from microspheres. Mansur et al. (2019) also reported that exendin-4 could significantly improve the collagen maturity and mineralized crystallinity to repair the damaged bone mass and mechanical properties in T2DM individuals. Further, the micro-CT analysis provided an accurate assessment for the bone microstructure around implants (Figure 4). The results showed that the drug released from carriers could improve the quantity and quality of bone around implants in diabetic rats. Kim et al. (2013) also reported that exendin-4 can protect the bone mineral density of femur in T2DM rats. Another study has also proposed that exendin-4 could improve bone mass and protect bone trabecular microstructure by promoting bone formation and suppressing bone resorption (Ma et al., 2013). Thus, it can be demonstrated that exendin-4 had a positive effect on bone around implants, which are crucial for the realization of better osseointegration in diabetes.

In addition, the histological analysis further confirmed that exendin-4-loaded microspheres can enhance the osseointegration in T2DM rats (Figure 6). Over the same period, normal rats showed obvious bone trabecula in contact with the surface of the implants, but there was nearly no newly formed bone at the implant-bone interface in the T2DM rats. T2DM contributes to a lower osseointegration, which may be caused by multiple factors, including the abnormal calcium and phosphorus metabolism (Liu et al., 2020; Zhao et al., 2020), hyperglycemia, AGEs, ROS, chronic inflammation, and the vicious cycle among them (Yamazaki et al., 2020). After drug intervention, the improved bone trabecula structure around implants and the better osseointegration could be observed. However, the specific mechanism still remains unclear. The reason might be related to the enhancement of exendin-4 on the osteogenesis capacity. It has been proved that the exenatide can improve the serum osteogenesis factor in diabetic rats (Zhou et al., 2015). Another study also reported that the systemically injected exenatide can significantly enhance the expression of fibronectin and integrin $\alpha5\beta1$ in diabetic rats (Liu et al., 2015), which can promote the adhesion of osteoblasts at the surface of titanium implants. These results all suggested that exendin-4 can act as positive signals to regulate osseointegration. However, the mechanism should be further elucidated, and the drug delivery process should be optimized. Significantly, the local application of drug-loaded microspheres did not affect the blood glucose significantly (Figure 3(E)), indicating that the beneficial effect of exendin-4 on osseointegration might be, in whole or in part, independent of blood glucose control.

This study mainly focused on the effect of local application of exendin-4 on osseointegration using drug-loaded microspheres. Thus, one limitation of this study is the negligence of the comparison of PLGA-formulated drugs and free drugs, which can increase the credibility of results. In the future further study, the comparison of PLGA-formulated drugs and free drugs would be performed.

5. Conclusions

In conclusion, diabetes will impair the bone tissue around implants and osseointegration, while the local application of exendin-4 has a positive effect on the peri-implant bone regeneration and osseointegration without affecting the blood glucose. The exendin-4-loaded chitosan–PLGA microspheres with good properties could be a viable and promising strategy to improve the clinical efficacy of dental implants in T2DM patients. But further studies are essential to provide more supporting evidence and elucidate the cellular and molecular mechanism before applying this production to human clinical trials.

Acknowledgements

The authors would like to thank the staff in the Department of Oral Implants, School of Stomatology, The Fourth Military Medical University for their help in this project.

Disclosure statement

The authors report no conflicts of interest related to this study.

Funding

This study was supported by the National Natural Science Foundation of China under Grant Numbers (81771107, 82170991). Key Research and Development Program of Shaanxi, China (Grant number: 2020SF-014).

Data availability statement

The data generated and analyzed during this study are available from corresponding author on reasonable request.

References

Abd El Hady WE, Mohamed EA, Soliman OAE, et al. (2019). In vitro–in vivo evaluation of chitosan–PLGA nanoparticles for potentiated gastric retention and anti-ulcer activity of diosmin. Int J Nanomedicine 14:7191–213.

Ahmad N, Ahmad R, Alrasheed RA, et al. (2020). A chitosan–PLGA based catechin hydrate nanoparticles used in targeting of lungs and cancer treatment. Saudi J Biol Sci 27:2344–57.

Apostu D, Lucaciu O, Lucaciu GD, et al. (2017). Systemic drugs that influence titanium implant osseointegration. Drug Metab Rev 49:92–104.

Arafa MG, Mousa HA, Afifi NN. (2020). Preparation of PLGA–chitosan based nanocarriers for enhancing antibacterial effect of ciprofloxacin in root canal infection. Drug Deliv 27:26–39.

Badran MM, Alomrani AH, Harisa GI, et al. (2018). Novel docetaxel chitosan-coated PLGA/PCL nanoparticles with magnified cytotoxicity and bioavailability. Biomed Pharmacother 106:1461–8.

Chen H, Xie LQ, Qin J, et al. (2016). Surface modification of PLGA nanoparticles with biotinylated chitosan for the sustained in vitro release and the enhanced cytotoxicity of epirubicin. Colloids Surf B Biointerfaces 138:1–9.

Chen MM, Cao H, Liu YY, et al. (2017). Sequential delivery of chlorhexidine acetate and bFGF from PLGA-glycol chitosan core-shell microspheres. Colloids Surf B Biointerfaces 151:189–95.

Chien CT, Jou MJ, Cheng TY, et al. (2015). Exendin-4-loaded PLGA microspheres relieve cerebral ischemia/reperfusion injury and neurologic deficits through long-lasting bioactivity-mediated phosphorylated Akt/eNOS signaling in rats. J Cereb Blood Flow Metab 35:1790–803.

Coelho PG, Pippenger B, Tovar N, et al. (2018). Effect of obesity or metabolic syndrome and diabetes on osseointegration of dental implants in a miniature swine model: a pilot study. J Oral Maxillofac Surg 76: 1677–87.

Deng B, Zhu W, Duan Y, et al. (2019). Exendin-4 promotes osteogenic differentiation of adipose-derived stem cells and facilitates bone repair. Mol Med Rep 20:4933–42.

Deng Y, Zhu W, Anhua L, et al. (2021). Exendin-4 promotes bone formation in diabetic states via HDAC1-Wnt/β-catenin axis. Biochem Biophys Res Commun 544:8–14.

Guo Q, Wang W, Abboud R, et al. (2020). Impairment of maturation of BMP-6 (35 kDa) correlates with delayed fracture healing in experimental diabetes. J Orthop Surg Res 15:186.

Jiang L, Zhang W, Wei L, et al. (2018). Early effects of parathyroid hormone on vascularized bone regeneration and implant osseointegration in aged rats. Biomaterials 179:15–28.

Kim J, Lee S, Jo K, et al. (2013). Exendin-4 increases bone mineral density in type 2 diabetic OLETF rats potentially through the down-regulation of SOST/sclerostin in osteocytes. Life Sci 92:533–40.

King S, Klineberg I, Levinger I, et al. (2016). The effect of hyperglycaemia on osseointegration: a review of animal models of diabetes mellitus and titanium implant placement. Arch Osteoporos 11:29.

Kuchler U, Spilka T, Baron K, et al. (2011). Intermittent parathyroid hormone fails to stimulate osseointegration in diabetic rats. Clin Oral Implants Res 22:518–23.

Lecka-Czernik B. (2017). Diabetes, bone and glucose-lowering agents: basic biology. Diabetologia 60:1163–9.

Li T, Chandrashekar A, Beig A, et al. (2021). Characterization of attributes and in vitro performance of exenatide-loaded PLGA long-acting release microspheres. Eur J Pharm Biopharm 158:401–9.

Liang Q, Du L, Zhang R, et al. (2021). Stromal cell-derived factor-1/exendin-4 cotherapy facilitates the proliferation, migration and osteogenic differentiation of human periodontal ligament stem cells in vitro and promotes periodontal bone regeneration in vivo. Cell Prolif 54:e12997.

Liu XX, Jiang L, Liu Q, et al. (2020). Low bone turnover markers in young and middle-aged male patients with type 2 diabetes mellitus. J Diabetes Res 2020:6191468.

Liu Z, Zhou W, Tangl S, et al. (2015). Potential mechanism for osseointegration of dental implants in Zucker diabetic fatty rats. Br J Oral Maxillofac Surg 53:748–53.

López-Gómez SA, González-López BS, Scougall-Vilchis RJ, et al. (2020). Tooth loss in patients with and without diabetes: a large-scale, cross-sectional study of Mexican adults. J Am Dent Assoc 151:276–86.

Lu B, Lv X, Le Y. (2019). Chitosan-modified PLGA nanoparticles for control-released drug delivery. Polymers 11:304.

Ma X, Meng J, Jia M, et al. (2013). Exendin-4, a glucagon-like peptide-1 receptor agonist, prevents osteopenia by promoting bone formation and suppressing bone resorption in aged ovariectomized rats. J Bone Miner Res 28:1641–52.

Mansur SA, Mieczkowska A, Flatt PR, et al. (2019). The GLP-1 receptor agonist exenatide ameliorates bone composition and tissue material properties in high fat fed diabetic mice. Front Endocrinol 10:51.

Meng J, Ma X, Wang N, et al. (2016). Activation of GLP-1 receptor promotes bone marrow stromal cell osteogenic differentiation through β-catenin. Stem Cell Rep 6:579–91.

Niang P, Ba A, Dia TS, et al. (2011). Diabetes mellitus and early failures in oral implantology. Odontostomatol Trop 34:26–32.

Nissen A, Marstrand S, Skov-Jeppesen K, et al. (2019). A pilot study showing acute inhibitory effect of GLP-1 on the bone resorption marker CTX in humans. JBMR Plus 3:e10209.

Pereira M, Gohin S, Roux J, et al. (2017). Exenatide improves bone quality in a murine model of genetically inherited type 2 diabetes mellitus. Front Endocrinol 8:327.

Pola CC, Moraes ARF, Medeiros EAA, et al. (2019). Development and optimization of pH-responsive PLGA–chitosan nanoparticles for triggered release of antimicrobials. Food Chem 295:671–9.

Qi F, Wu J, Yang T, et al. (2014). Mechanistic studies for monodisperse exenatide-loaded PLGA microspheres prepared by different methods based on SPG membrane emulsification. Acta Biomater 10:4247–56.

Sanna V, Roggio AM, Pala N, et al. (2015). Effect of chitosan concentration on PLGA microcapsules for controlled release and stability of resveratrol. Int J Biol Macromol 72:531–6.

Sanz C, Vázquez P, Blázquez C, et al. (2010). Signaling and biological effects of glucagon-like peptide 1 on the differentiation of mesenchymal stem cells from human bone marrow. Am J Physiol Endocrinol Metab 298:E634–E43.

Schiellerup SP, Skov-Jeppesen K, Windeløv JA, et al. (2019). Gut hormones and their effect on bone metabolism. Potential drug therapies in future osteoporosis treatment. Front Endocrinol 10:75.

Sun H, Lu N, Liu D, et al. (2016). The bone-preserving effects of exendin-4 in ovariectomized rats. Endocrine 51:323–32.

Taghavi S, Ramezani M, Alibolandi M, et al. (2017). Chitosan-modified PLGA nanoparticles tagged with 5TR1 aptamer for in vivo tumor-targeted drug delivery. Cancer Lett 400:1–8.

Takeuchi I, Takeshita T, Suzuki T, et al. (2017). Iontophoretic transdermal delivery using chitosan-coated PLGA nanoparticles for positively charged drugs. Colloids Surf B Biointerfaces 160:520–6.

Wang N, Gao J, Jia M, et al. (2017). Exendin-4 induces bone marrow stromal cells migration through bone marrow-derived macrophages polarization via PKA-STAT3 signaling pathway. Cell Physiol Biochem 44:1696–714.

Wang P, Zhuo X, Chu W, et al. (2017). Exenatide-loaded microsphere/thermosensitive hydrogel long-acting delivery system with high drug bioactivity. Int J Pharm 528:62–75.

Wang X, Qi F, Xing H, et al. (2019). Uniform-sized insulin-loaded PLGA microspheres for improved early-stage peri-implant bone regeneration. Drug Deliv 26:1178–90.

Yamazaki S, Masaki C, Nodai T, et al. (2020). The effects of hyperglycaemia on peri-implant tissues after osseointegration. J Prosthodont Res 64:217–23.

Zhao H, Qi C, Zheng C, et al. (2020). Effects of glycated hemoglobin level on bone metabolism biomarkers in patients with type 2 diabetes mellitus. Diabetes Metab Syndr Obes 13:1785–91.

Zhou H, Li D, Shi C, et al. (2015). Effects of exendin-4 on bone marrow mesenchymal stem cell proliferation, migration and apoptosis in vitro. Sci Rep 5:12898.

Zhou W, Liu Z, Yao J, et al. (2015). The effects of exenatide microsphere on serum BGP and ALP levels in ZDF rats after implantation. Clin Implant Dent Relat Res 17:765–70.